Article

Discovery Medicine 2026; 38(205): 587–596
https://doi.org/10.24976/Discov.Med.202638205.48

Computed Tomography-Based Radiomics Model for Predicting KIT Exon 11 Codons 557–558 Deletion Mutation in Gastrointestinal Stromal Tumors

Caijuan Zhang[1], Qing Song[2], Jingyu Wang[2], Dong Dong[2], Weiling Xu[2,*]

[1]Department of Radiology, The Fourth Affiliated Hospital of School of Medicine, and International School of Medicine, International Institutes of Medicine, Zhejiang University, 322000 Yiwu, Zhejiang, China

[2]Department of Radiology, The First Hospital of Jilin University, 130021 Changchun, Jilin, China

*Correspondence: xuweiling@jlu.edu.cn (Weiling Xu)

Submitted: 26 November 2025 Revised: 20 January 2026 Accepted: 23 January 2026 Published: 20 February 2026

Background: Gastrointestinal stromal tumors (GISTs) are common mesenchymal tumors with significant variations in prognosis and sensitivity to imatinib. Traditional detection of the DEL 557–558 mutation requires invasive procedures and is costly. Radiogenomics, by analyzing imaging, can predict tumor mutations and provide diagnostic and prognostic insight. Based on this, this study constructs and validates a radiomics-based prediction framework to preoperatively identify the KIT exon 11 codon 557–558 deletion mutation (DEL 557–558) in GISTs using contrast-enhanced CT (CE-CT).

Methods: The CE-CT images and medical record data were examined for 126 GIST patients who underwent surgical resection and gene mutation testing between 2019 and 2021 at the medical center. Optimal radiomic features were extracted from the selected region of interest (ROI) on the CE-CT images. Two logistic regression (LR) models were established to forecast DEL 557–558: one utilized solely radiomic features, while the other incorporated both radiomic and clinicopathological parameters. The effectiveness of the LR models' predictions was assessed through receiver operating characteristic (ROC) curve analysis, with the mean area under the curve (AUC) value calculated via a five-fold cross-validation protocol.

Results: Gastric location, higher mitotic count and higher Ki-67 expression were associated with GIST patients with DEL 557–558 mutation. The radiomic features model, incorporating 12 radiomic features, had AUCs of 0.90 $\pm$ 0.01 (95% CI: 0.87–0.94), 0.76 $\pm$ 0.04 (95% CI: 0.66–0.88), 0.892 (95% CI: 0.824–0.960) and 0.850 (95% CI: 0.720–0.980) in the prediction of DEL 557–558 in the training, validation, cross-validation and test datasets, respectively. The integrated model combining radiomic attributes with clinicopathological parameters displayed enhanced predictive performance, achieving AUC values of 0.93 $\pm$ 0.01 (95% CI: 0.90–0.96), 0.82 $\pm$ 0.04 (95% CI: 0.71–0.91), 0.916 (95% CI: 0.857–0.974) and 0.875 (95% CI: 0.745–1.000) in the training, validation, cross-validation and test datasets, respectively.

Conclusion: Radiomics models may help predict DEL 557–558 mutations, thereby enabling more effective treatment selection and prognosis assessment.

Keywords: gastrointestinal stromal tumors; KIT; codon 557–558 deletion mutation; radiomics

Introduction

Gastrointestinal stromal tumors represent the predominant type of mesenchymal growths found within the gastrointestinal tract [1]. Gastrointestinal stromal tumors (GISTs) demonstrate diverse clinical manifestations, ranging in malignancy potential and sensitivities to imatinib medication treatment in individual patients [2,3].

The commonly used risk stratification model for GISTs was established based on tumor size, tumor location (gastric or non-gastric), and mitotic count [4]. Furthermore, it has been shown that GISTs with different mutations hold a strong influence on prognostic results and responses to imatinib [5]. A stratification of GISTs into three categories based on gene mutation detection: "c-KIT", "PDGFRA" and "wild-type", showed that mutations in the c-KIT proto-oncogene, were the most common mutation type (80%–85%), and were sensitive to tyrosine kinase inhibitor (TKI) imatinib [5]. However, GIST patients with KIT exon 11 codons 557–558 deletion mutation (named 'DEL 557–558'), displayed heightened aggressive clinical characteristics and elevated secondary resistance toward imatinib [6,7]. It has been reported that medium-risk GISTs with DEL 557–558 showed similar prognostic results to high-risk tumor patients with other gene mutation types [6]. Other studies' results have also strongly suggested that GIST patients harboring DEL 557–558 were associated with shorter progression-free survival (PFS) [8,9]. This data holds specific significance in the context of adjuvant therapy, where an accurate prediction of GISTs carry-

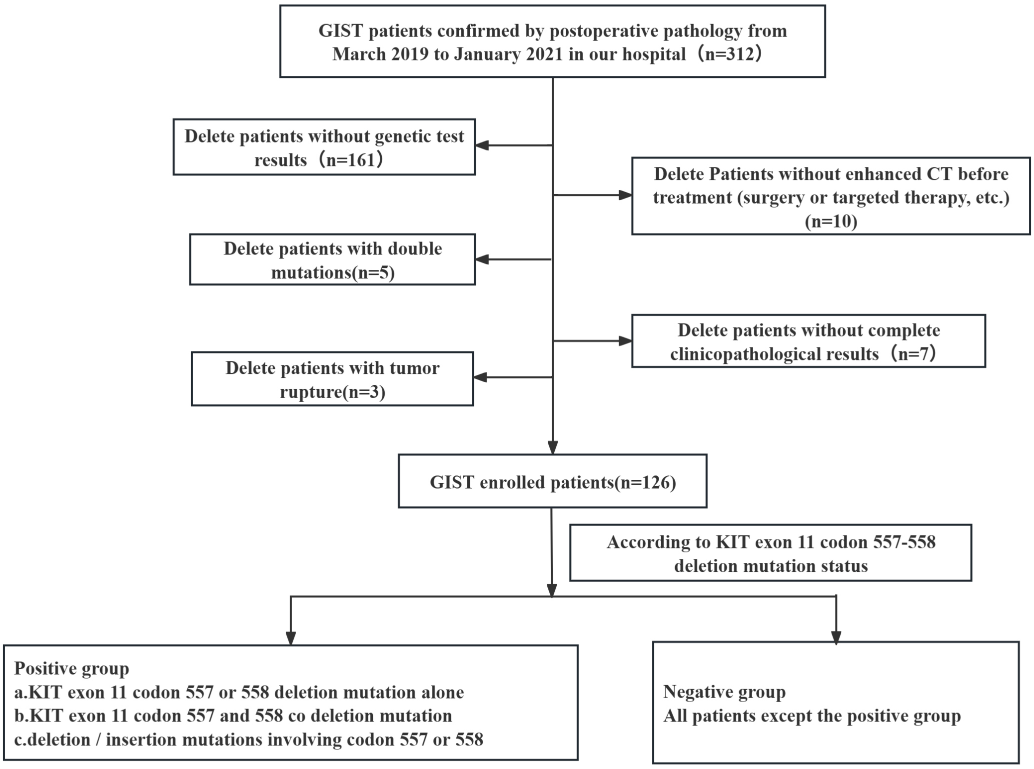

Fig. 1. Workflow chart with respect to patient recruitment. GIST, gastrointestinal stromal tumor; CT, computed tomography.

ing DEL 557–558 mutation could assist in better identifying tumors with a higher risk of and earlier relapse, and guide clinical decision-making.

The conventional method to detect the 557–558 deletion mutation relies on surgical specimens or biopsy samples obtained invasively before surgical operations. Furthermore, given the heterogeneous nature of tumor samples, the detection of DEL 557–558 based on invasive biopsy is not sufficient to represent the entire GISTs. Cost consideration also limits the broad application of genotype testing.

Radiogenomics, a method used for detecting the mutation status of a tumor based on imaging analysis, has gained wide recognition owing to providing additional results for the diagnosis, treatment decision-making and prognostication of tumours [10]. In the past decade, radiogenomics has emerged as a valuable approach across diverse tumor investigations, encompassing lung cancer, kidney cancer, prostate cancer and breast cancer, leading to the development of imaging biomarkers associated with genomic phenotypes, thus advancing precision medicine [11–14]. In this paper, we built and validated two radiomics models using multivariate CT features and clinicopathological data to predict DEL 557–558 in gastrointestinal stromal tumors.

Methods

Patient Selection

A cohort of 126 patients diagnosed with GISTs following postoperative pathology between March 2019 and January 2021 were selected for this retrospective analysis. The selection criteria included: (a) complete abdominal contrast-enhanced computed tomography (CE-CT) examination performed within 15 days prior to surgical intervention, (b) the genomic phenotype were detected by Sanger sequencing, (c) the patients who had complete clinicopathological information. The exclusion criteria included: (a) the patients who underwent surgery or targeted therapy before CT examination, (b) those that presented with double mutation, (c) patients whose tumor ruptured during the surgery. (d) Patients without genetic test results, (e) Patients without complete clinicopathological results. The selection procedure for patients is illustrated in Fig. 1.

The included patients were divided into positive group and negative group according to the DEL 557–558 status. The positive group included those with: (1) KIT exon 11 codon 557 or 558 deletion mutation alone; (2) KIT exon 11 codon 557 and 558 deletion mutation together; (3) deletion/insertion mutations involving codon 557 or 558. The remaining patients were assigned to the negative group.

Training Set: About 70% of the total data, that is, 88 out of 126 cases were used for model training, accounting. During training, the model automatically adjusts its internal parameters by learning the features and label relationships in the training set to optimize performance.

Independent evaluation team: ① Validation Set: This dataset was used for hyperparameter tuning during model training and it accounted for 15% of the total data, that is, 19 out of 126 cases (the actual value is approximated according to the proportion, and adjusted to 19 cases within the 70%: 15%:15% ratio for ease of calculation and operation). Evaluating the model's performance under different hyperparameter combinations in the validation set aided the selection of the optimal hyperparameter settings to improve the model's generalizability. ② Test Set: This accounted for 15% of the total data, that is, 19 out of 126 cases. It was used for independently evaluating the final model after training and validation tuning, to objectively reflect the model's performance in real-world applications.

CT Protocol

All subjects underwent imaging using PHILIPS iCT 64/256-detector spiral CT and Siemens 16/64-detector spiral CT systems. The scanning parameters encompassed: tube voltage at 120 kV; tube current of 300 mA; pitch ratio of 0.9; matrix size of 512 $\times$ 512; and slice thickness ranging from 1–1.5 mm. During dynamic contrast-enhanced CT examination, iopromide contrast medium (85 mL) was administered intravenously at 2.5 mL/s. The sequential imaging was performed to acquire arterial phase (25–30 s), venous phase (60 s), and equilibrium phase (180 s) scans.

Feature Extraction and Selection

In this investigation, CT images of each lesion were assessed independently by two certified radiologists, and all CT images were anonymized. The two radiologists initially evaluated CT imaging features, including tumor location (gastric or non-gastric), tumor size (maximum transverse diameter), shape (regular or irregular), edge contour (clear or fuzzy), ulcer (presence or absence), intratumoral degeneration (necrosis or cystic transformation), and enhancement mode (uniform or uneven). Interobserver agreement between the two readers for each finding was calculated using an independent samples *t* test

Next, the CT images were exported to the ITK-SNAP software (version3.8.0; http://www.itksnap.org) in Digital Imaging and Communication in Medicine format, and then three-dimensional (3D) segmentation of the region of interest (ROI) was executed by the two radiologists. Feature extraction and selection were conducted in pyradiomics (V3.0.1, https://pyradiomics.readthedocs.io/en/latest/) and RIAS [15,16]. From each GIST's 3D ROI, radiomic features were procured, encompassing (I) wavelet transform; (II) first-order texture feature; (III) shape features; (IV) gray-level co-occurrence matrix (GLCM); (V) gray-level size-zone matrix (GLSZM); (VI) gray-level run-length matrix (GLRLM); (VII) neighborhood graytone difference matrix (NGTDM); and (VIII) gray-level dependence matrix (GLDM). Initially, radiomics features with $p < 0.05$ were identified through *t*-test analysis. Subsequently, these features underwent further filtering utilizing least absolute shrinkage and selection operator (LASSO). The agreement of features extraction was assessed through inter- and intraclass correlation coefficients (ICCs). Agreement was considered satisfactory when ICC exceeded 0.75.

Radiomics Model Building

Two logistic regression (LR) models were established for DEL 557–558 prediction: radiomic features model and radiomic features combined with clinicopathological features model. The dataset was arbitrarily split into a cross-validation cohort and a test cohort, with a 7:3 proportion. The model parameters were optimized through a 5-fold cross-validation procedure using the cross-validation dataset. Subsequently, the prediction capability of the radiomics model underwent evaluation within the test cohort.

Statistical Analysis

Statistical analysis was performed using SPSS26.0 (SPSS Inc., Chicago, IL, USA). The Shapiro-Wilk test was employed for normality testing. For normally distributed continuous data (age), descriptive statistics were presented as $\bar{X} \pm$ S. Independent sample *t*-tests were used for comparisons, and F test was used for multiple groups. Non-normally distributed data was represented with quartiles as MQ2 (Q1, Q3), and analyzed with the Mann-Whitney U test. Count data (general clinical data, CT morphological features and pathological features) were expressed as frequencies or rates, and comparisons were conducted with χ^2 test or Fisher's exact test. Statistical significance was established at $p < 0.05$. The assessment of the radiomics model's effectiveness employed receiver operating characteristic (ROC) curves. The discriminative capability of the radiomics model was determined through multiple metrics, encompassing the area under the curve (AUC), sensitivity, specificity, positive predictive value (PPV), and negative predictive value (NPV). Collinearity was diagnosed using variance inflation factors (VIF), and Pearson correlation analysis was used for correlation analysis.

Results

Clinicopathological Data Analysis

In this study, the 126 GIST patients consisted of 68 males (58.53 $\pm$ 11.32 years) and 58 females (57.17 $\pm$ 11.03 years). Of the total patients, 36 patients had KIT exon 11 codon 557–558 deletion mutation, with the mutation rate accounting for 28.6%. In the Training Set, descriptive statistics showed that gastric location, mitotic count, Ki-67, were associated with the KIT exon 11 codon 557–558 deletion mutation (p = 0.028, 0.001, 0.007, respectively). There was no significant difference between Age, Gender, Tumor diameter, shape, Malignant potential and CD34 ($p > 0.05$) (Table 1).

Radiomics Features Extraction and Selection

The consistency of feature extraction through ICC were first assessed, and only the features with ICC values exceeding 0.75 and $p < 0.05$ were retained. A total of 1427 features were obtained from the GIST patients' data. To control for false discovery rate (FDR) caused by multiple

Table 1. Clinical and pathological data analysis of GIST patients.

Clinicopathological features	Training Set (n = 88)		$Z/t/x^2$	p	Independent evaluation team (n = 38)		$Z/t/x^2$	p
	KIT exon 11 codon 557–558 deletion mutation				KIT exon 11 codon 557–558 deletion mutation			
	Positive	Negative			Positive	Negative		
No. of patients	26	62	-	-	10	28	-	-
Age	55.50 ± 11.91	58.90 ± 11.65	1.241	0.218	50.70 ± 9.91	60.50 ± 8.50	2.998	0.005*
Gender								
Male	16 (61.54)	34 (54.84)	0.335	0.563	5 (50.00)	13 (46.43)	-	1.000
Female	10 (38.46)	28 (45.16)			5 (50.00)	15 (53.57)		
Tumor location								
Gastric	20 (76.92)	32 (51.61)	4.854	0.028*	6 (60.00)	15 (53.57)	-	1.000
No-gastric	6 (23.08)	30 (48.39)			4 (40.00)	13 (46.43)		
Tumor diameter								
≤5 cm	9 (34.62)	18 (29.03)	0.269	0.604	2 (20.00)	14 (50.00)	-	0.143
>5 cm	17 (65.38)	44 (70.97)			8 (80.00)	14 (50.00)		
Shape								
Regular	10 (38.46)	32 (51.61)	1.270	0.260	4 (40.00)	13 (46.43)	-	1.000
Irregular	16 (61.54)	30 (48.39)			6 (60.00)	15 (53.57)		
Malignant potential								
Very low risk	0 (0.00)	0 (0.00)	-	0.209	0 (0.00)	2 (7.14)	-	0.498
Low risk	1 (3.85)	10 (16.13)			1 (10.00)	6 (21.43)		
Medium risk	9 (34.62)	17 (27.42)			1 (10.00)	5 (17.86)		
High risk	16 (61.54)	35 (56.45)			8 (80.00)	15 (53.57)		
Mitotic count								
≤5 HPF	6 (23.08)	40 (64.52)	12.609	0.001*	5 (50.00)	22 (78.57)	-	0.116
>5 HPF	20 (76.92)	22 (35.48)			5 (50.00)	6 (21.43)		
CD34								
Positive	24 (92.31)	49 (79.03)	1.441	0.230	0 (0.00)	5 (17.86)	-	0.298
Negative	2 (7.69)	13 (20.97)			10 (100.00)	23 (82.14)		
Ki-67								
<10%	13 (50.00)	49 (79.03)	7.417	0.007*	6 (60.00)	20 (71.43)	-	0.694
≥10%	13 (50.00)	13 (20.97)			4 (40.00)	8 (28.57)		

*$p < 0.05$, the difference was statistically significant.

GIST, Gastrointestinal stromal tumor; HPF, High-Power Field.

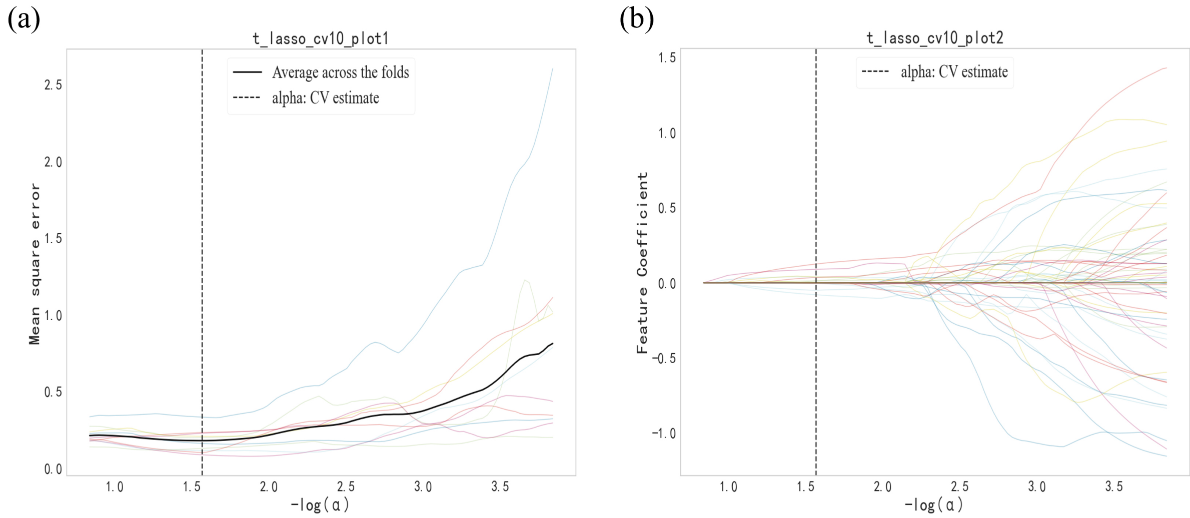

Fig. 2. Multivariable selection of radiomic features based on LASSO regression. (a) The fine dotted lines display individual LASSO regularized curves for each fold, while the bold continuous line indicates the averaged curve from LASSO 5-fold cross-validation. A vertical broken line marks the (–log(α)) position that corresponds to the optimal α value when minimal mean square error occurs. The determined α value reached 0.0271. (b) The delicate dotted lines represent feature coefficient values per fold across various –log(α) measurements, and the vertical broken line signifies the (–log(α)) position corresponding to the optimal α value, yielding 12 features with non-zero characteristic coefficients. LASSO, least absolute shrinkage and selection operator.

tests, we introduced a Benjamin-Hochberg (BH) procedure to ensure the authenticity of the selected features. Subsequently, the LASSO algorithm combined with five-fold cross verification was used to screen out 12 groups of radiomic feature patterns (Fig. 2). Specifically, the alpha value was determined by minimizing the cross-validation MSE and the final value was 0.0271. In order to reduce the risk of overfitting, based on the 12 sets of features screened by LASSO, we further used elastic network regularization to enhance the stability of the model, and finally verified the 12 sets of features. To assess the correlation between the final 12 features, we calculated the VIF and the correlation matrix. The results showed that the VIF values for all features were less than 5 and the absolute value of the Pearson correlation coefficient was less than 0.7, indicating that there was no significant multicollinearity between the features. See Table 2 for the specific names and corresponding coefficients of these 12 sets of characteristic models.

Development of the Prediction Models

The radiomics features model was constructed with 12 selected radiomic characteristics to predict the KIT exon 11 codon 557–558 deletion mutation utilizing five-fold cross-validation. The primary parameters established in the LR classifier included solver = ‘liblinear’, tol = 0.0001, C = 1.0. According to the analytical outcomes (Fig. 3), the prediction model exhibited AUC values of 0.90 $\pm$ 0.01 (95% CI: 0.87–0.94) in training, 0.76 $\pm$ 0.04 (95% CI: 0.66–0.88) in validation, 0.892 (95% CI: 0.824–0.960) in cross-validation, and 0.850 (95% CI: 0.720–0.980) in the test dataset.

The integrated model incorporating the radiomics features alongside clinical-pathological parameters was constructed similarly by combining the 12 selected radiomics features, 3 clinicopathological features (tumor location, mitotic count and Ki-67), Lasso-score and Rad-score. The model had AUC of 0.93 $\pm$ 0.01 (95% CI: 0.90–0.96), 0.82 $\pm$ 0.04 (95% CI: 0.71–0.91), 0.916 (95% CI: 0.857–0.974) and 0.875 (95% CI: 0.745–1.000) in predicting the deletion of KIT exon 11 codons 557–558 in the training, validation, cross-validation and test dataset, respectively (Fig. 4).

The calculation formula of Lasso-score and Rad-score in the fusion LR model was:

Lasso-Score=exponential_glrlm_RunLengthNonUniformity*(0.0120)+log-sigma-1-0-mm-3D_firstorder_Uniformity*(0.0386)+log-sigma-1-0-mm-3D_glszm_SmallAreaEmphasis*(0.0127)+log-sigma-3-0-mm-3D_firstorder_InterquartileRange*(–0.0039)+log-sigma-3-0-mm-3D_firstorder_Energy*(0.08945)+original_firstorder_InterquartileRange*(–0.0008)+wavelet-LLH_firstorder_Energy*(0.0393)+wavelet-LLH_glrlm_ShortRunLowGrayLevelEmphasis*(0.1246)+wavelet-LHL_gldm_LargeDependenceLowGrayLevelEmphasis*(–0.0796)+wavelet-LHH_glszm_LargeAreaHighGrayLevelEmphasis*(0.0351)+wavelet-HLL_glszm_LargeAreaEmphasis*(0.0024)+wavelet-LLL_firstorder_InterquartileRange(–0.0502)

Rad-score=–1.1325+exponential_glrlm_RunLengthNonUniformity*(0.2781)+log-sigma-1-0-mm-3D_firstorder_Uniformity*(0.6018)+log-sigma-1-0-mm-3D_glszm_SmallAreaEmphasis*(0.0784)+log-sigma-3-0-mm-3D_firstorder_InterquartileRange*(0.0085)+log-sigma-3-0-mm-3D_firstorder_Energy*(0.8582)+original_firstorder_Interq

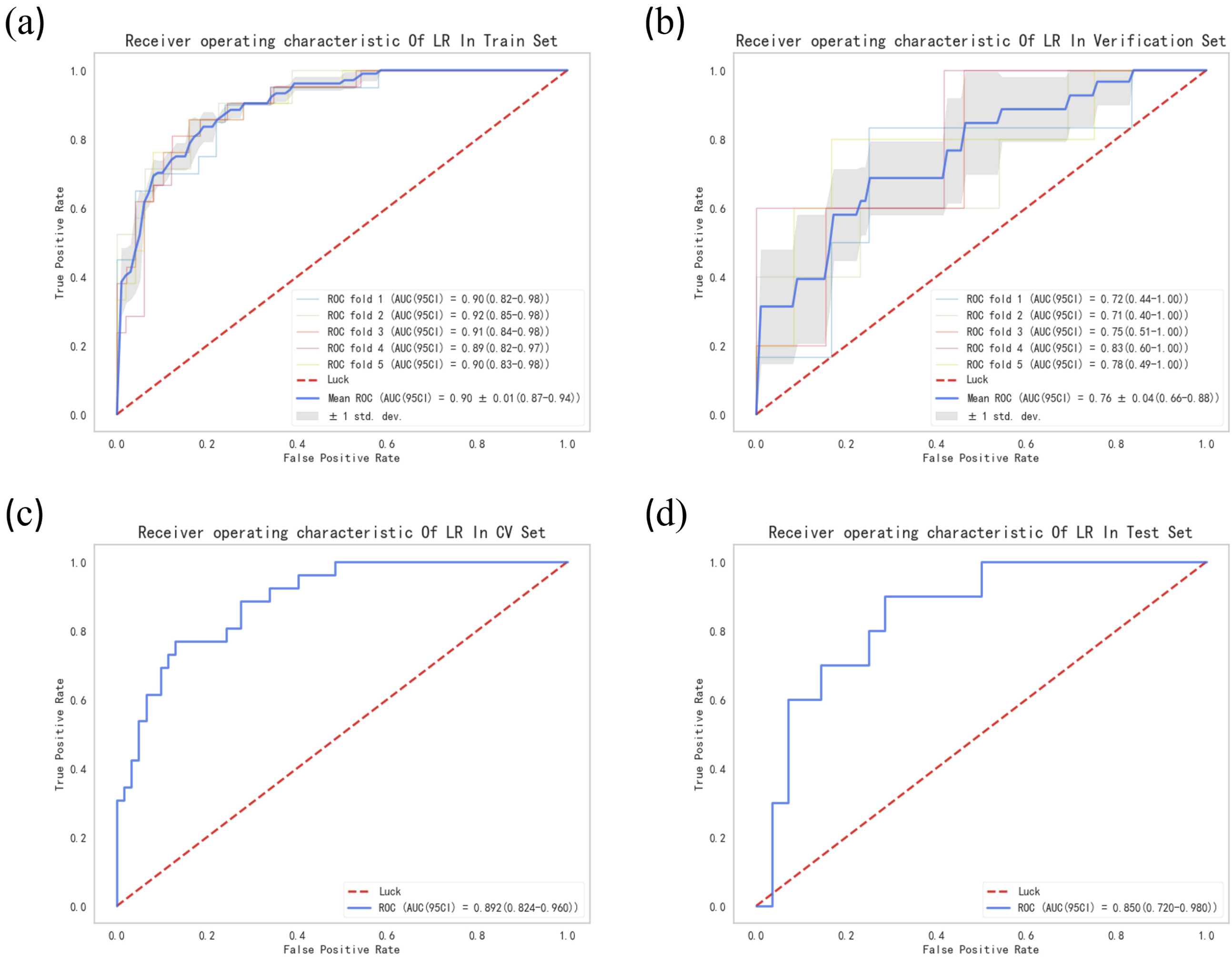

Fig. 3. ROC curves of training (a), validation (b), the cross-validation (c), and test datasets (d) for the radiomics model. (a) Training ROC curve: This curve reflects the performance of the model on the training data set. The AUC value of the training set is 0.90 ± 0.01, which shows the model's high ability to fit on the training data, that is, the model can well capture the relationship between the features in the training data and the target variables. (b) Validation ROC curve: This curve is used to evaluate the generalizability of the model on an independent validation data set. The AUC value of the validation set was 0.76 ± 0.04, which was slightly lower than the training set, but still showed that the model had certain predictive power on unseen data. (c) Cross-validation ROC curve: This curve shows the performance of the model during the five-fold cross-validation process. Through multiple cross-validation, the calculated AUC value was 0.892, indicating that the model has high prediction accuracy during the cross-validation process. (d) Test datasets ROC curve: This curve shows the performance of the model on the final test data set. The AUC value of the test set is 0.850, indicating that the model has good predictive ability in practical application scenarios. ROC, receiver operating characteristic curve; AUC, area under the curve.

uartileRange*(–0.2726)+wavelet-LLH_firstorder_Energy*(–0.0168)+wavelet-LLH_glrlm_ShortRunLowGrayLevelEmphasis*(1.1682)+wavelet-LHL_gldm_LargeDependenceLowGrayLevelEmphasis*(–1.0999)+wavelet-LHH_glszm_LargeAreaHighGrayLevelEmphasis*(0.0531)+wavelet-HLL_glszm_LargeAreaEmphasis*(0.1299)+wavelet-LLL_firstorder_InterquartileRange(–0.3837)

To evaluate the classification effectiveness of the radiomics model, the diagnostic metrics comprising sensitivity, specificity, PPV, and NPV were computed and presented (Table 3).

Discussion

The development of GISTs genotypes have shifted the treatment paradigm [8,17]. Detecting particular mutations in GISTs now represent an essential component of patient care strategies and selection of adjuvant therapies. GIST patients carrying DEL 557–558 mutation have less favorable RFS and develop secondary resistance more rapidly than those with mutations other than DEL 557–558. Consequently, therapeutic planning for GIST cases presenting this specific deletion requires consideration of both the imple-

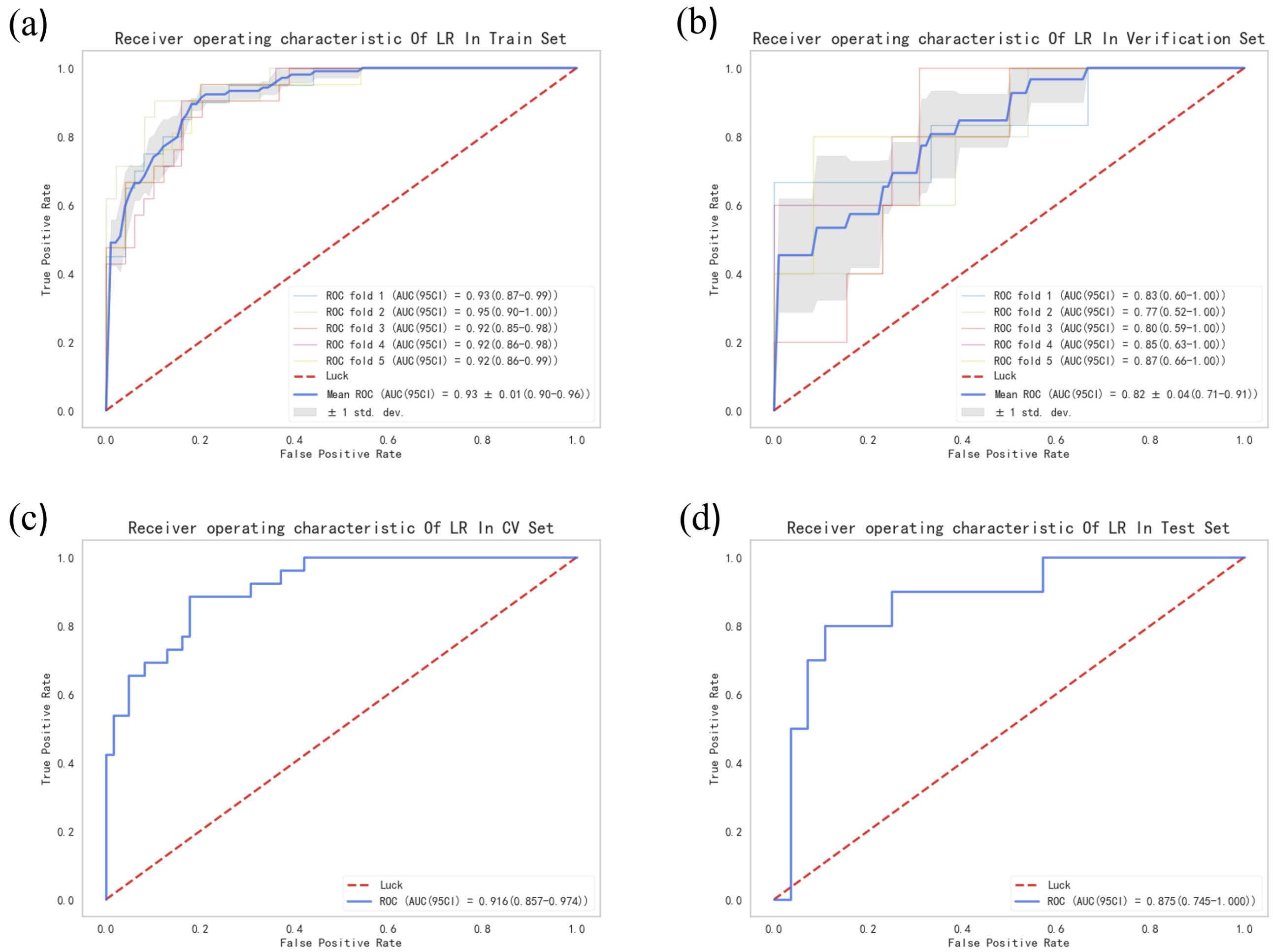

Fig. 4. ROC curves of training (a), validation (b), the cross-validation (c), and test datasets (d) for the fusion model. (a) The ROC curve of the training set shows that the AUC value is 0.93 ± 0.01, reflecting that the model has excellent fitting effect on training data and is better than the radiomic characteristic model alone. (b) The ROC curve of the validation shows that the AUC value is 0.82 ± 0.04, indicating that the model has strong generalizability on the independent validation data set and has improved prediction performance compared with the individual model. (c) The ROC curve of the cross-validation shows that the AUC value is 0.916, indicating a high prediction stability and accuracy in cross-validation. (d) The ROC curve of the test datasets shows that the AUC value is 0.875, which proves that the model has higher prediction accuracy and reliability in practical applications.

Table 2. Names and coefficients of non-zero radiomics features.

Name	Coefficients
exponential_glrlm_RunLengthNonUniformity	0.0120
log-sigma-1-0-mm-3D_firstorder_Uniformity	0.0386
log-sigma-1-0-mm-3D_glszm_SmallAreaEmphasis	0.0127
log-sigma-3-0-mm-3D_firstorder_InterquartileRange	–0.0039
log-sigma-3-0-mm-3D_firstorder_Energy	0.08945
original_firstorder_InterquartileRange	–0.0008
wavelet-LLH_firstorder_Energy	0.0393
wavelet-LLH_glrlm_ShortRunLowGrayLevelEmphasis	0.1246
wavelet-LHL_gldm_LargeDependenceLowGrayLevelEmphasis	–0.0796
wavelet-LHH_glszm_LargeAreaHighGrayLevelEmphasis	0.0351
wavelet-HLL_glszm_LargeAreaEmphasis	0.0024
wavelet-LLL_firstorder_InterquartileRange	–0.0502

Table 3. Accuracy of DEL 557–558 predicted by the two models in the training, validation, cross-validation and test cohort.

Model	Dataset	Sensitivity	Specificity	PPV	NPV
Radiomics model	Train set	0.75 ± 0.04	0.85 ± 0.02	0.68 ± 0.05	0.89 ± 0.02
	validation set	0.59 ± 0.15	0.75 ± 0.14	0.51 ± 0.12	0.81 ± 0.07
	cross-validation set	0.73	0.87	0.70	0.89
	Test set	0.70	0.86	0.64	0.89
Fusion model	Train set	0.87 ± 0.04	0.83 ± 0.02	0.68 ± 0.03	0.94 ± 0.02
	validation set	0.69 ± 0.09	0.75 ± 0.13	0.56 ± 0.14	0.85 ± 0.03
	cross-validation set	0.85	0.82	0.67	0.93
	Test set	0.80	0.89	0.73	0.93

PPV, positive predictive value; NPV, negative predictive value.

mentation and duration of adjuvant imatinib administration. The present investigation established and validated two robust predictive frameworks for determining DEL 557–558 status, utilizing radiomics features and clinicopathological parameters.

Recent studies have focused extensively on investigating how distinct KIT exon 11 mutation patterns and locations influence RFS outcomes, and developing an effective radiomics model to predict the genotypes [18–20]. Xu *et al*. [20] successively trained a cross-validation SVM classifier used to identify GISTs lacking KIT exon 11 mutation (AUC = 0.864–0.904). Our study is the first to analyze the relevant radiomic and clinicopathological features on DEL 557–558 and construct a predictive model of the critical deletions. The results showed that the radiomics features model alone, and the radiomics features combined with clinicopathological features model could effectively predict DEL 557–558 with AUC of 0.850 and 0.875 in the test cohorts, respectively. Although no notable ROC curve differences emerged between these LR models, the integrated approach incorporating clinicopathological features exhibited superior sensitivity, specificity, PPV, and NPV compared to the radiomics features model alone. The lack of notable ROC curve differences between these LR models may be resolved by collecting more data in the future, as some clinicopathological features showed statistical significance.

In this study, the age of deletion-mutation-positive group in the test cohort was younger than that of the negative group (p = 0.005), which may have resulted from differences in grouping. The gastric location, higher mitotic count and higher Ki-67 expression had strong relevance in the GIST patients with DEL 557–558, which aligns with findings from earlier research and substantiates the suggestion that DEL 557–558 correlates with aggressive tumor characteristics [6,21]. However, some studies showed that gender and tumor diameter were significantly correlated with codon 557–558 deletion mutation [6,7], which was not observed in our study, nor in another report [9]. Therefore, the significance of tumor diameter remains uncertain.

GIST patients presenting with DEL 557–558 are not uncommon, the mutation rate usually ranges from 15%–40% of cases [22,23]. In our dataset, the mutation rate of DEL 557–558 accounted for 28.6%. Some scholars have proposed that tumor genotype should be considered as a new risk stratification variable, including the mutation of DEL 557–558 [22]. In recent years, resistance to imatinib has emerged as a major challenge in the adjuvant treatment of GIST. Our findings could contribute to the identification of GIST patients with DEL 557–558 as they represent the most suitable target for investigating resistance to adjuvant therapy.

The current investigation faced several constraints. First, the results showed that there were differences between the training set and the independent verification set in key clinical characteristics such as age, tumor location, mitotic count, and Ki-67. Such inconsistencies could cause the model to overfit specific feature distributions in the training set during training, while in the verification set, prediction performance may be degraded due to feature differences, i.e., the risk of "over-matching". This bias may obscure the true generalization of the model and affect the reliability of extrapolating results to other populations. Therefore, future studies need to mitigate these issues through strict data stratification, feature balancing or increasing sample size.

Also, the sample size was limited as the study encompassed a sum of 126 participants, with 88 individuals allocated to the cross-validation cohort and 38 subjects designated to the test cohort. The limited sample size may primarily be due to the high cost of genetic testing, which creates economic pressure for large-scale patient data collection. The ability to conduct this study under limited resource conditions indicates that the proposed method has favorable cost-effectiveness characteristics, making it closer to actual clinical application scenarios. However, a small sample size brings several issues. It may lead to insufficient model training, and failure to fully capture the intricate features and patterns of the data, thus raising doubts about the model's generalizability, i.e., the model's predictive accuracy on new data may decrease. Moreover, it may also not sufficiently represent the characteristics of the entire gastrointestinal stromal tumor patient population, posing a risk of sample bias and affecting the reliability and universality of the research results. Nevertheless, despite this issue, this study still provides a foundation and direction for subsequent related research and offers exploratory insights.

Second, our data mainly originated from a single center and lacked external validation. Third, the information on patients' prognosis was not available. In the future, we will follow up these patients and collect their prognostic information to further verify the prognostic impact of codon 557–558 deletion mutation. Finally, this study relied on AUC/ROC to evaluate the model. AUC/ROC focuses on the model's discriminative ability but cannot reflect the agreement between predicted probabilities and actual occurrence probabilities, that is, calibration. Future research needs to further include calibration analysis and decision curve analysis to more comprehensively assess the model's clinical utility.

Conclusion

This study used a model constructed with radiomics features and integrated clinicopathological parameters with good predictive value for KIT gene exon 11 codon 557–558 deletion mutations prediction in gastrointestinal stromal tumors. The integrated model performed better and is expected to help clinicians identify patients at higher risk of recurrence earlier, guide personalized treatment decisions, and has potential clinical applicability.

Availability of Data and Materials

The analyzed data sets generated during the study are available from the corresponding author upon reasonable request.

Author Contributions

CZ drafted and edited manuscript. CZ and WX formulated the research framework. QS and DD executed the research and evaluated the data. WX revised the manuscript, while JW supervised the study and compiled the data and figures. All authors have been involved in revising it critically for important intellectual content. All authors gave final approval of the version to be published. All authors have participated sufficiently in the work to take public responsibility for appropriate portions of the content and agreed to be accountable for all aspects of the work in ensuring that questions related to its accuracy or integrity.

Ethics Approval and Consent to Participate

This investigation follows the guidelines specified in the Declaration of Helsinki. The research was approved by the Medical Ethics Committee of the First Hospital of Jilin University (approval number: 20241191). Given the retrospective design of this investigation, the committee determined that informed consent requirements could be waived. We have de-identified all patient details to ensure the confidentiality of patient information.

Acknowledgment

Not applicable.

Funding

This research received no external funding.

Conflict of Interest

The authors declare no conflict of interest.

References

[1] Rubin BP, Heinrich MC, Corless CL. Gastrointestinal stromal tumour. Lancet (London, England). 2007; 369: 1731–1741. https://doi.org/10.1016/S0140-6736(07)60780-6.

[2] Yoo C, Ryu MH, Ryoo BY, Beck MY, Kang YK. Efficacy, safety, and pharmacokinetics of imatinib dose escalation to 800 mg/day in patients with advanced gastrointestinal stromal tumors. Investigational New Drugs. 2013; 31: 1367–1374. https://doi.org/10.1007/s10637-013-9961-8.

[3] Shah R, Jonnalagadda S. The GIST of a stromal tumor. Gastroenterology. 2005; 128: 2170–2172. https://doi.org/10.1053/j.gastro.2005.03.086.

[4] Joensuu H. Risk stratification of patients diagnosed with gastrointestinal stromal tumor. Human Pathology. 2008; 39: 1411–1419. https://doi.org/10.1016/j.humpath.2008.06.025.

[5] Oppelt PJ, Hirbe AC, Van Tine BA. Gastrointestinal stromal tumors (GISTs): point mutations matter in management, a review. Journal of Gastrointestinal Oncology. 2017; 8: 466–473. https://doi.org/10.21037/jgo.2016.09.15.

[6] Incorvaia L, Badalamenti G, Fanale D, Vincenzi B, Luca ID, Algeri L, *et al*. Not all *KIT* 557/558 codons mutations have the same prognostic influence on recurrence-free survival: breaking the exon 11 mutations in gastrointestinal stromal tumors (GISTs). Therapeutic Advances in Medical Oncology. 2021; 13: 17588359211049779. https://doi.org/10.1177/17588359211049779.

[7] Wardelmann E, Losen I, Hans V, Neidt I, Speidel N, Bierhoff E, *et al*. Deletion of Trp-557 and Lys-558 in the juxtamembrane domain of the c-kit protooncogene is associated with metastatic behavior of gastrointestinal stromal tumors. International Journal of Cancer. 2003; 106: 887–895. https://doi.org/10.1002/ijc.11323.

[8] Patrikidou A, Domont J, Chabaud S, Ray-Coquard I, Coindre JM, Bui-Nguyen B, *et al*. Long-term outcome of molecular subgroups of GIST patients treated with standard-dose imatinib in the BFR14 trial of the French Sarcoma Group. European Journal of Cancer (Oxford, England: 1990). 2016; 52: 173–180. https://doi.org/10.1016/j.ejca.2015.10.069.

[9] Martin-Broto J, Gutierrez A, Garcia-Del-Muro X, Lopez-Guerrero JA, Martinez-Trufero J, de Sande LM, *et al*. Prognostic time dependence of deletions affecting codons 557 and/or 558 of KIT gene for relapse-free survival (RFS) in localized GIST: a Spanish Group for Sarcoma Research (GEIS) Study. Annals of Oncology: Official Journal of the European Society for Medical Oncology. 2010; 21: 1552–1557. https://doi.org/10.1093/annonc/mdq047.

[10] Rutman AM, Kuo MD. Radiogenomics: creating a link between molecular diagnostics and diagnostic imaging. European Journal of Radiology. 2009; 70: 232–241. https://doi.org/10.1016/j.ejrad.2009.01.050.

[11] Pinker K, Chin J, Melsaether AN, Morris EA, Moy L. Preci-

sion Medicine and Radiogenomics in Breast Cancer: New Approaches toward Diagnosis and Treatment. Radiology. 2018; 287: 732–747. https://doi.org/10.1148/radiol.2018172171.
[12] Karlo CA, Di Paolo PL, Chaim J, Hakimi AA, Ostrovnaya I, Russo P, *et al*. Radiogenomics of clear cell renal cell carcinoma: associations between CT imaging features and mutations. Radiology. 2014; 270: 464–471. https://doi.org/10.1148/radiol.13130663.
[13] Lu X, Li M, Zhang H, Hua S, Meng F, Yang H, *et al*. A novel radiomic nomogram for predicting epidermal growth factor receptor mutation in peripheral lung adenocarcinoma. Physics in Medicine and Biology. 2020; 65: 055012. https://doi.org/10.1088/1361-6560/ab6f98.
[14] Ferro M, de Cobelli O, Vartolomei MD, Lucarelli G, Crocetto F, Barone B, *et al*. Prostate Cancer Radiogenomics-From Imaging to Molecular Characterization. International Journal of Molecular Sciences. 2021; 22: 9971. https://doi.org/10.3390/ijms22189971.
[15] Li M, Li X, Guo Y, Miao Z, Liu X, Guo S, *et al*. Development and assessment of an individualized nomogram to predict colorectal cancer liver metastases. Quantitative Imaging in Medicine and Surgery. 2020; 10: 397–414. https://doi.org/10.21037/qims.2019.12.16.
[16] van Griethuysen JJM, Fedorov A, Parmar C, Hosny A, Aucoin N, Narayan V, *et al*. Computational Radiomics System to Decode the Radiographic Phenotype. Cancer Research. 2017; 77: e104–e107. https://doi.org/10.1158/0008-5472.CAN-17-0339.
[17] Joensuu H, Wardelmann E, Sihto H, Eriksson M, Sundby Hall K, Reichardt A, *et al*. Effect of KIT and PDGFRA Mutations on Survival in Patients With Gastrointestinal Stromal Tumors Treated With Adjuvant Imatinib: An Exploratory Analysis of a Randomized Clinical Trial. JAMA Oncology. 2017; 3: 602–609. https://doi.org/10.1001/jamaoncol.2016.5751.
[18] Incorvaia L, Fanale D, Vincenzi B, De Luca I, Bartolotta TV, Cannella R, *et al*. Type and Gene Location of *KIT* Mutations Predict Progression-Free Survival to First-Line Imatinib in Gastrointestinal Stromal Tumors: A Look into the Exon. Cancers. 2021; 13: 993. https://doi.org/10.3390/cancers13050993.
[19] Bachet JB, Hostein I, Le Cesne A, Brahimi S, Beauchet A, Tabone-Eglinger S, *et al*. Prognosis and predictive value of KIT exon 11 deletion in GISTs. British Journal of Cancer. 2009; 101: 7–11. https://doi.org/10.1038/sj.bjc.6605117.
[20] Xu F, Ma X, Wang Y, Tian Y, Tang W, Wang M, *et al*. CT texture analysis can be a potential tool to differentiate gastrointestinal stromal tumors without KIT exon 11 mutation. European Journal of Radiology. 2018; 107: 90–97. https://doi.org/10.1016/j.ejrad.2018.07.025.
[21] Wozniak A, Rutkowski P, Schöffski P, Ray-Coquard I, Hostein I, Schildhaus HU, *et al*. Tumor genotype is an independent prognostic factor in primary gastrointestinal stromal tumors of gastric origin: a european multicenter analysis based on ConticaGIST. Clinical Cancer Research: an Official Journal of the American Association for Cancer Research. 2014; 20: 6105–6116. https://doi.org/10.1158/1078-0432.CCR-14-1677.
[22] Martín J, Poveda A, Llombart-Bosch A, Ramos R, López-Guerrero JA, García del Muro J, *et al*. Deletions affecting codons 557-558 of the c-KIT gene indicate a poor prognosis in patients with completely resected gastrointestinal stromal tumors: a study by the Spanish Group for Sarcoma Research (GEIS). Journal of Clinical Oncology: Official Journal of the American Society of Clinical Oncology. 2005; 23: 6190–6198. https://doi.org/10.1200/JCO.2005.19.554.
[23] Dematteo RP, Gold JS, Saran L, Gönen M, Liau KH, Maki RG, *et al*. Tumor mitotic rate, size, and location independently predict recurrence after resection of primary gastrointestinal stromal tumor (GIST). Cancer. 2008; 112: 608–615. https://doi.org/10.1002/cncr.23199.